PHOTOCATHODE STUDIES FOR ULTRA-LOW-EMITTANCE ELECTRON SOURCES

K.C. Harkay†, Y. Li, K. Nemeth, R.A. Rosenberg, M. White, ANL, Argonne, IL 60439, U.S.A *
L.K. Spentzouris, Illinois Institute of Technology, Chicago, IL 60616, U.S.A **

Abstract

Future x-ray sources, such as FELs and ERLs, impose very demanding requirements on the emittance and bunch repetition rate of the electron source. Even if perfect compensation of space-charge effects could be attained, the fundamental physics of cathode emission sets a lower bound on achievable source emittance. Development of ultra-low-emittance sources is a rapidly evolving area of R&D with exciting new results achieved at low bunch charge. However, it is very difficult to compare different results and to quantify what works. The study and optimization of low-emittance photocathodes is still limited in scope. In this paper, we describe an R&D effort to systematically design optimized photocathodes that are suitable for an FEL or ERL, and to measure their fundamental properties. The status and results to date are reported.

MOTIVATION

High-brightness electron sources are critical in meeting the demanding requirements of future x-ray energy recovery linac (XERL) [1-3] and free-electron laser (XFEL) [4-7] sources. State-of-the-art FEL electron injectors give about 1 nC bunch charge with 1 mm-mr emittance normalized to the beam energy, and operate at 120 Hz or less. The goal for future XFELs (high-coherence mode [1]) and the XFEL oscillator (XFELO) [7] is about 0.1 mm-mr normalized emittance with lower bunch charge but with repetition rates of 1 MHz or more (see Fig. 1). High-brightness sources are, therefore, a rapidly evolving area of R&D for ERL/FEL applications. There are promising designs using alternative cathodes, VHF rf cavities, and pulsed DC [6,9] as well as important advances in beam dynamics and photocathode gun design. Exciting new results were recently reported by PSI [10], SLAC/LCLS [4], Cornell, and U. Maryland on injectors at low charge with ultra-low emittance. The majority of the effort is on injectors using conventional photocathodes: metal or semiconductors.

Even in the case of large bunch charge and perfect emittance compensation, the fundamental cathode emittance is an important contribution to the ultimate beam brightness; this is supported by simulations [11,12]. In more recent work, the maximum achievable brightness depends only on the applied field and the intrinsic (also called "thermal") emittance, independent of bunch charge [13]. The intrinsic emittance depends on the emitted momentum distribution, the surface roughness, nonuniformity, and impurities (e.g., oxide layers), grain boundaries, and the laser energy and polarization. The challenge is to combine all of the relevant phenomena into a complete and useful physical model [14]. It is difficult to compare the results from different labs and quantify what works. The study of fundamental emission properties is limited in scope, with work at Naval Research Lab–U. of Maryland; Tsinghua U.–POSTECH–BNL; INFN Milan; LBNL–Brescia; SLAC; and JLab.

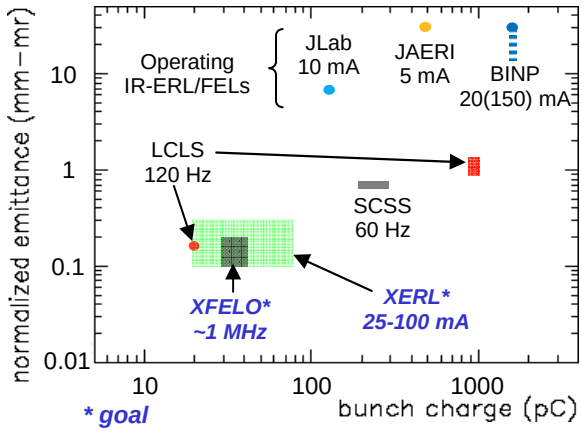

Figure 1: ERL and FEL injector performance or goals [1-8].

We plan to systematically measure the fundamental material properties of suitable candidate photocathodes and then design materials with photoemission properties optimized for ultra-low emittance. The effort is divided into two parts. Experimentally, we will apply surface analysis techniques in the lab to characterize photocathode surfaces and then correlate material properties with emittance. Theoretically, we will calculate electron band structures for crystal surfaces using density functional theory (DFT) analysis [15] and then estimate the transverse momentum distribution using the three-step photoemission model [16]. Material designs that predict small emittance will be investigated experimentally.

EXPERIMENT

Angle-resolved photoemission spectroscopy (ARPES) is an important tool in the study of electronic structure of crystals [17]. In the photoemission process, the surface-parallel momentum is conserved which, in accelerator terminology, corresponds to the transverse momentum. For initial investigations, we assume the simplest case where there is no electron-electron scattering [18]; therefore, the angular energy distribution of electrons photoemitted from a sample surface is correlated with the momentum distribution of electronic states in the crystal. In conventional ARPES, the photon energies are in the 20- to 100-eV range. We are planning to use UV photons

* Work supported by U. S. Department of Energy, Office of Science, Office of Basic Energy Sciences, under Contract No. DE-AC02-06CH11357.
** Work supported by National Science Foundation Grant No. 0237162.
† harkay@aps.anl.gov

in the 4- to 6-eV range, close to the work function of many typical cathode materials, to measure the momentum distribution of photoelectrons at emission.

The apparatus being assembled for the ARPES measurements is shown in Fig. 2. The samples under study will be located in an ultra-high vacuum (UHV) chamber made with mu-metal to shield external magnetic fields (marked "A" in the figure). Samples are loaded into the sample introduction chamber (marked "B") and introduced into the analysis chamber using a transfer arm (not shown). Samples are mounted on holders and can be heated to ~1000 C or cooled to ~140 K. A laser will illuminate the sample through a port indicated with an arrow in Fig. 2. A UV flashlamp (broad spectrum) and UV laser (Nd:YAG, 266 nm) will be used for calibration and quantitative measurements, respectively. Energy is measured by a time-of-flight (TOF) electron detector based on a pair of microchannel plates (MCPs). The detector is mounted on a flange inside the chamber on a mechanical assembly that allows it to rotate with respect to the sample. By rotating both the sample and the detector, the angular distribution of emitted electrons can be measured. The chamber also has an x-ray photoemission spectroscopy (XPS) system allowing the sample surface chemistry to be measured. The chamber layout and ProE CAD model are presently being optimized. Final drawings will be used to support detailed physics simulations of the electron transport and for component assembly.

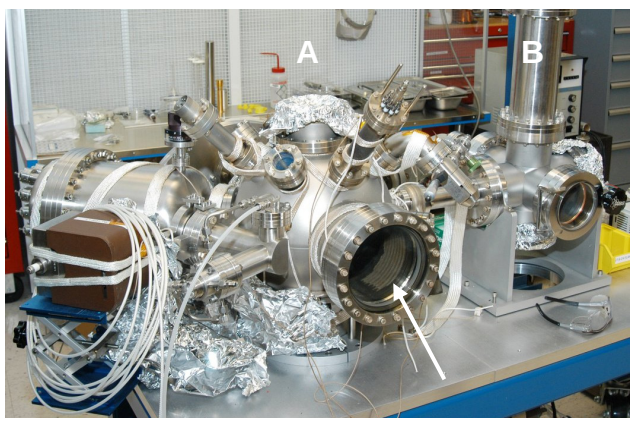

Figure 2: UHV analysis chamber (A) and sample introduction chamber (B). The laser and TOF detector assembly will be mounted on the flange indicated by the arrow.

The threshold angular resolution required for the photoemission experiments is derived from a normalized transverse emittance goal of 0.1 mm-mrad. In practice the photocathode intrinsic emittance must be smaller than this, since it adds in quadrature to other sources of error. The normalized emittance is defined as

$$\varepsilon_{n,\mathrm{int}} = \beta\sqrt{\langle x^2\rangle\langle x'^2\rangle} = \beta\sigma_x\sigma_{x'}. \qquad (1)$$

The position and momentum are assumed to be uncorrelated and γ=1 at emission; β is the relative velocity. Note that $\sigma_x^2 = \langle x^2\rangle$ is taken to be the size of the laser spot on the cathode surface. The angle of a photoelectron is $x' = \arcsin(p_x/p)$ and $p = \sqrt{2mE_k} = m\beta c$ is the total momentum (E_k is the kinetic energy). Then, the photoelectron distribution must be measured to determine $\sigma_{x'}^2 = \langle x'^2\rangle = \arcsin(\sigma_{p_x}/p)$.

An important goal of the experimental study is to verify theoretical predictions of the beam emittance based on σ_{p_x} obtained from electronic band structure calculations. Well-studied metallic crystals will be characterized first, including Cu(111) and Cu(001), followed by other crystals with favorable calculated properties (work function and emission momentum distribution).

THEORY

We plan to calculate electronic band structures for crystal surfaces and then estimate the transverse momentum using the three-step photoemission model [16]. For a surface model, a surface slab of 4, 8, or 16 layers (L) with 2D periodic boundary conditions (along the surface lattice vectors) is constructed and the band structure and work functions ϕ computed using the plane-waves DFT code PWSCF [19]. For such a model, the electronic bands represent the dispersion relation of the electronic energy of single-electron states over the surface-parallel momenta. The bands are periodic with the surface periodicity, thus only their representation in the Brillouin zone is given. Calculated dispersion relations for the energy bands of silver (001) are shown on the left side of Fig. 3.

The surface bands are the highest-energy partially occupied bands that fall below the Fermi level E_f only for limited regions of the momentum-space. The electronic states of these surface bands are usually well localized in the vicinity of the surface. The electrons occupying such a region of allowed k-space require the least energy to overcome the work function and escape the material as photoelectrons. If the laser energy is high enough to liberate these electrons, but cannot reach the next energy band, no other electrons will be emitted. The right side of Fig. 3 shows the range in k_x-space of electrons in the surface band. The dark blue region represents the occupied states below E_f. The required value of $\sigma_{p_x} = \hbar k_{\max}$ for an intrinsic emittance calculation may thus be obtained from the computed band structure.

The band structure and ϕ were computed for several crystals: Cu(001), Cu(111), Ag(001), and Ag(111). Table 1 gives ϕ, k_{max}, and corresponding intrinsic emittances (using Eq. 1). For ϕ, the agreement between the calculated and experimental [20,21] values is 9-13%. This accuracy is consistent with other DFT ϕ calculations for various metals [22]. For k_{max}, the agreement with other calculations [23] is within 8-13%. This gives us confidence in applying this method to other candidate photocathodes.

It is convenient to describe the intrinsic emittance in terms of a "thermal" energy, E_{th}: $\varepsilon_{n,th} = \sigma_x\sqrt{2E_{th}/3mc^2}$ [24]. We can compute the effective thermal energy for the

crystals in Table 1 using the intrinsic emittance from Eq. (1) and assuming σ_x is 0.3 mm. Table 1 lists the results.

Initial investigations were made of MgO monolayers on Ag, a well-studied material in catalysis [25]. DFT computations suggest that the surface-parallel momenta in the surface band for this system are well limited. Comparison of Figs. 3 and 4 shows the significant changes in k_{max} when two MgO monolayers (2L) are added on Ag (4L). The >1-eV reduction in the computed work function (see Table 1) is suggestive of negative electron affinity cathodes (others have also applied thin layers to control ϕ [26]). The analysis suggests a design method for other thin-layered photocathodes. Estimation of the photoelectron yield is under development.

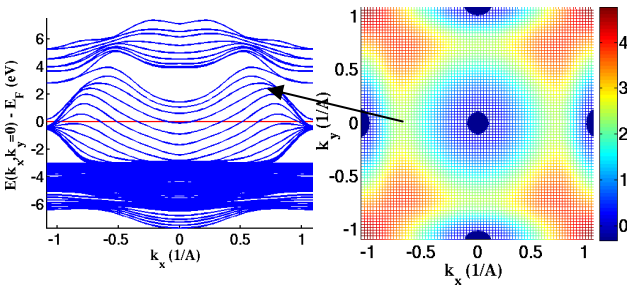

Figure 3: Ag(001)16L; DFT(PBE). Left: k_x vs. energy bands relative to E_f. Right: Lowest surface band in k_x vs. k_y space.

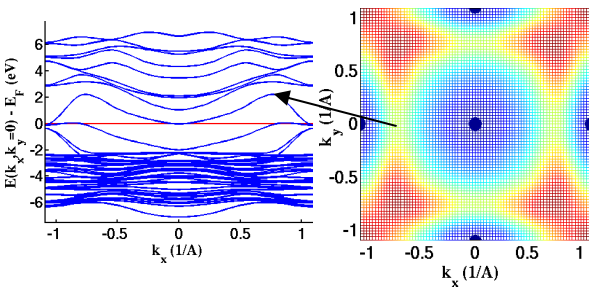

Figure 4: MgO(100)2L-Ag(100)4L-MgO(100)2L; DFT (PW91). Computed work function reduced by >1 eV relative to Fig. 3.

Table 1: Computed Properties of Various Crystals

Surface *	Computed ϕ (eV)	Experimental ϕ (eV) **	k_{max} (1/Å)	k_{offset} (1/Å)	E_{th} (eV)	$\varepsilon_{n,int}$*** (mm-mr)
Cu(001)	4.18	4.59	0.15	0	0.27	0.18
Cu(001)	4.18	4.59	0.03	1.229	–	*>9.92 eV needed*
Cu(111)	4.36	4.94	0.25	0	1.09	0.36
Ag(001)	4.06	4.64	0.10	0	0.12	0.12
Ag(001)	4.06	4.64	0.07	1.087	–	*> 8.55 eV needed*
Ag(111)	4.17	4.74	0.11	0	0.14	0.13
Thin film	2.92	2.92	0.05	0	0.029	0.06
Thin film	2.92	2.92	0.05	1.087	–	*>7.41 eV needed*

* Metal (16L) and thin-film (MgO(100)2L-Ag(100)4L-MgO(100)2L) slabs

** Photoemission experimental values for Cu, Ag [20,21]; independent calculation for layered structure [25].

*** Eq. (1); σ_x=0.3 mm, hν = 4.66 eV (266 nm) Nd:YAG

We have implemented a simple method of calculating ARPES spectra on the basis of DFT band structures following the recipe of Smith [21, Chapter 6.3] that is based on the three-step model. The code provides relative emission probabilities as a function of emission angles and emitted electron kinetic energy for input values of photon energy, polarization, ϕ, and band structure. The effect of the electron-electron scattering is included. Preliminary results on moderately discretized (8×8×3) k-space qualitatively give the same emission pattern (for Cu(001) and MgO2L-Ag4L-MgO2L) obtainable by simple analysis of surface bands. Higher k-space resolution is needed to obtain finer (<1 deg) angular resolution.

ACKNOWLEDGEMENTS

The authors wish to acknowledge H. Padmore, W. Wan, M. Van Veedendaal, and K. Attenkofer for generous advice and valuable discussions. The use of computational resources at NERSC (DOE DE-AC02-05CH11231) is gratefully acknowledged.

REFERENCES

[1] I.V. Bazarov et al., Proc. PAC 2001, 230 (2001); G. Hoffstaetter, http://fls2006.desy.de (2006).
[2] M. White, Y. Cho, http://srf2003.desy.de/fap/paper/MOP42.pdf (2003).
[3] M. Borland, G. Decker, A. Nassiri, Y. Sun, M. White, Nucl. Instrum. Methods A 582, 54 (2007).
[4] R. Akre et al., Phys. Rev. ST Accel. Beams 11, 030703 (2008); R. Akre et al., Proc. 2008 FEL Conf. (MOPPH052).
[5] European XFEL, http://xfel.eu/.
[6] K. Togawa et al., Phys. Rev. ST Accel. Beams 10, 020703 (2007); T. Shintake, Proc. EPAC 2006, 2741 (2006).
[7] K.-J. Kim, Y. Shvyd'ko, S. Reiche, Phys. Rev. Lett. 100, 244802 (2008).
[8] A. Todd, Nucl. Instrum. Methods A 557, 36 (2005).
[9] P. Ostroumov, K.-J. Kim, P. Piot, Proc. LINAC08 (TUP117).
[10] R. Ganter et al., Phys. Rev. Lett. 100, 064801 (2008).
[11] I.V. Basarov, C.K. Sinclair, Phys. Rev. ST Accel. Beams 8, 034202 (2005).
[12] Y.-e Sun et al., Proc. LINAC 2008 (TUP100).
[13] I.V. Basarov, B.M. Dunham, C.K. Sinclair, Phys. Rev. Lett. 102, 104801 (2009).
[14] K.-J. Kim, ed., Report No. ANL/APS/LS-305 (2004).
[15] A. Michaelides, M. Scheffler, in K. Wandelt, ed., *Surface and Interface Science*, Vol. I (Vch Pub) (2009).
[16] W.E. Spicer, A. Herrera-Gomez, SLAC-PUB-6306 (1993).
[17] A. Damascelli, Physica Scripta T109, 61 (2004).
[18] H. Padmore, W. Wan, "A Note on the Emittance of Surface State Electrons," LBNL Note (Jan 29, 2007).
[19] P. Giannozzi et al., http://www.quantum-espresso.org.
[20] CRC Handbook, 83rd edition (2003).
[21] M. Cardona, L. Ley eds., *Photoemission in Solids I*, (Springer-Verlag) (1985).
[22] Y. Ikuno, K. Kusakabe, e-J. Surf. Sci. Nanotech. 6, 103 (2008).
[23] S.D. Kevan, Phys. Rev. Lett. 50, 526 (1983); S.D. Kevan, R.H. Gaylord, Phys. Rev B 36, 5809 (1987); S.D. Kevan, Phys. Rev. B 28, 2268 (1983).
[24] K. Flöttmann, TESLA FEL-Report 1997-01.
[25] L. Giordano et. al., Physical Chem. Chemical Phys. 8, 3335 (2006).
[26] U. Martinez, L. Giordano, G. Pacchioni, J. Chem. Phys. 128, 164707 (2008).